Astronomy & Astrophysics manuscript no. output
May 6, 2026

Dissecting Ruprecht 147: A Bayesian 4D analysis of stellar rotation and binarity

Constraints from differentiable PARSEC isochrones and *Gaia* data release 3

Huanbin Chi[1,2], Feng Wang[2], Xuefen Tian[1]⋆, and Xiaoyun Zhu[1]

[1] School of Artificial Intelligence, Yunnan Open University, Kunming 650599, China
e-mail: chihuanbin@126.com
[2] Center for Astrophysics, Guangzhou University, Guangzhou 510006, China

Received Month Day, Year; accepted Month Day, Year

ABSTRACT

Context. Open clusters are fundamental benchmarks for calibrating stellar evolution models. However, the precise determination of cluster parameters is often hindered by the broadening of the main sequence due to unresolved binaries and stellar rotation, particularly near the main-sequence turnoff (MSTO). Ruprecht 147, as the oldest ($\sim$ 2.5 Gyr) and nearest ($d \sim 300$ pc) open cluster, provides a unique opportunity to resolve these degeneracies.
Aims. We aim to simultaneously constrain the fundamental parameters (age, metallicity, distance, and extinction) and the underlying population properties (binary fraction and rotational distribution) of Ruprecht 147 using a rigorous statistical framework that explicitly models the "Kraft break" in stellar rotation.
Methods. We constructed a 4D differentiable emulator based on PARSEC v2.0 stellar evolutionary tracks, utilizing `JAX` for GPU-accelerated inference. This emulator continuously interpolates mass, age, metallicity, and rotation rate (ω). We performed a hierarchical Bayesian analysis on high-precision *Gaia* data release 3 photometry using the No-U-Turn Sampler (NUTS) to sample the high-dimensional posterior distribution.
Results. Our analysis yields a precise distance modulus of $(m - M)_0 = 7.416^{+0.003}_{-0.002}$ mag and an age of $\tau = 2.340 \pm 0.002$ Gyr. We derive a super-solar metallicity of [M/H] $= +0.087^{+0.001}_{-0.003}$ dex. The inferred rotation distribution shape parameters ($\alpha_{\rm rot} \approx 7.9, \beta_{\rm rot} \approx 5.1$) indicate a mean rotation rate of $\bar{\omega} \approx 0.46$ for turnoff stars. We find a photometric binary fraction of $f_{\rm bin} \approx 33.9\%$.
Conclusions. The application of differentiable programming enables the robust breaking of the age-metallicity-extinction degeneracy. The detection of rapid rotation at the MSTO confirms the inefficiency of magnetic braking for stars with thin convective envelopes (the Kraft break), even at an advanced age of 2 Gyr. Its high metallicity suggests that Ruprecht 147 likely originated in the inner Galactic disk and migrated to its current location.

Key words. open clusters and associations: individual: Ruprecht 147 – stars: fundamental parameters – stars: rotation – stars: binaries: general – methods: statistical

1. Introduction

Open clusters serve as primary laboratories for stellar astrophysics. The assumption that cluster members share a common age, distance, and chemical composition enables rigorous testing of stellar evolution theories. Precise astrometric and photometric data from the *Gaia* mission (Gaia Collaboration et al. 2016, 2018, 2023a) have catalyzed a renaissance in open cluster studies, with thousands of new candidates identified in recent years (e.g., Cantat-Gaudin et al. 2018, 2020; Castro-Ginard et al. 2018, 2020). Our previous contributions to this field (Chi et al. 2023a,b,c, 2024, 2025; Chi & Wang 2025) have systematically characterized numerous newly discovered clusters. However, the color-magnitude diagrams (CMDs) of open clusters are rarely simple isochrones. They are broadened by observational uncertainties, differential extinction, unresolved binaries, and stellar rotation (Bastian & Lardo 2018).

The "extended main-sequence turnoff" (eMSTO) phenomenon highlights the importance of stellar rotation, which alters the hydrostatic equilibrium and surface temperature of stars (Brandt & Huang 2015). For intermediate-age clusters such as Ruprecht 147, the turnoff mass ($\sim$1.5–1.6 $M_\odot$) lies near the "Kraft break" (Kraft 1967; Beyer & White 2024), the transition zone where stars lose their thick convective envelopes and thus their magnetic braking efficiency.

Ruprecht 147 (NGC 6774) is a critical benchmark in this context. Despite its proximity ($d \approx 300$ pc), its parameters have been debated, with age estimates ranging from 2.5 to 3.0 Gyr (Curtis et al. 2020). In this work, we go beyond traditional grid-based isochrone fitting. We employed a hierarchical Bayesian framework using `JAX` to build a differentiable emulator of the PARSEC stellar models. This allowed us to sample the posterior distribution of cluster parameters while explicitly marginalizing the rotational and binary properties of individual stars.

As the oldest ($\sim$2.5–3.0 Gyr) and nearest open cluster, Ruprecht 147 holds exceptional promise as a standard for fundamental stellar astrophysics (Curtis et al. 2013). Its proximity enables detailed studies of stellar rotation, binary populations, and chemical abundances that are inaccessible for more

⋆ Corresponding author: 18382204138@163.com

Article published by EDP Sciences, to be cited as https://doi.org/10.1051/0004-6361/202659486

distant clusters of comparable age. The cluster's turnoff mass (∼1.5–1.6 $M_\odot$) places it precisely at the Kraft break (Kraft 1967; Beyer & White 2024), where stars lose their thick convective envelopes and consequently experience inefficient magnetic braking. This makes Ruprecht 147 an ideal laboratory for investigating the rotational evolution of intermediate-mass stars on gigayear timescales (Curtis et al. 2020). Recent high-resolution spectroscopy has established a super-solar metallicity of [Fe/H] ≈ +0.08 dex (Bragaglia et al. 2018), while dynamical studies reveal that the cluster is undergoing rapid dissolution, having lost ∼ 99% of its initial mass through tidal interactions with the Milky Way (Yeh et al. 2019). These characteristics—a well-determined chemical composition, measurable rotation periods spanning F- to M-type dwarfs (Curtis et al. 2020), and ongoing dynamical evolution—establish Ruprecht 147 as a cornerstone for testing gyrochronology relations, atomic diffusion processes (Liu et al. 2019), and the chemical enrichment history of the Galactic disk.

This work is organized as follows. In Sect. 2, we introduce the Gaia data release 3 (DR3) data and our quality selection criteria. Subsequently, we detail our methodology: first, we used HDBSCAN to identify cluster members; then, we built a differentiable stellar emulator; and finally, we applied a hierarchical Bayesian model to infer cluster parameters, accounting for binaries and rotation. In Sect. 4, we present the derived parameters of Ruprecht 147—including its age, distance, metallicity, binary fraction, and rotation distribution—and discuss their astrophysical implications. In Sect. 5, we summarize our conclusions.

2. Membership determination

2.1. Data selection and cleaning

We leveraged data from *Gaia* DR3 (Gaia Collaboration et al. 2023b). Initial candidates were selected within a radius of 3° centered on Ruprecht 147 ($(\alpha, \delta) = (289.1°, -16.3°)$). To ensure a pristine sample for isochrone fitting, we applied the following criteria.

1. Astrometry: We selected high-probability members based on proper motion clustering ($\mu_\alpha^* \approx -1.0, \mu_\delta \approx -27.0$ mas yr^{-1}) and parallax cuts ($2.5 < \varpi < 4.5$ mas).
2. Photometry: We restricted our sample to stars with photometric errors $\sigma_G < 0.02$ mag to minimize observational scatter.
3. Quality: We filtered out sources with a large renormalised unit weight error (RUWE > 1.4) to reject unresolved astrometric binaries or spurious solutions.

After applying these cuts, we retained $N_{\rm star} = 1\,234$ high-confidence members. Photometric uncertainties were taken from the Gaia catalog, and a zero-point offset of +0.017 mas was added to the parallaxes following Lindegren et al. (2021).

2.2. Cluster member selection with HDBSCAN

We employed the HDBSCAN (Hierarchical Density-Based Spatial Clustering of Applications with Noise) algorithm Campello et al. (2013); McInnes et al. (2017) to automatically identify cluster members from the Gaia DR3 astrometric data. HDBSCAN extends the DBSCAN algorithm Ester et al. (1996) by incorporating a hierarchical approach, enabling the identification of clusters with varying densities. This makes it particularly suitable for astrophysical applications where cluster boundaries may not be uniformly dense.

To optimize clustering performance, we implemented a systematic grid search over the hyperparameter space. The search encompassed:

- a minimum cluster size, varied from 5 to 50 in increments of 5;
- minimum samples, tested in the range 1–20;
- a cluster selection epsilon explored between 0.1 and 2.0.

The feature space for clustering consisted of the 5D astrometric parameter vector: $(\alpha, \delta, \varpi, \mu_{\alpha^*}, \mu_\delta)$, where $\mu_{\alpha^*} = \mu_\alpha \cos\delta$. Prior to clustering, all parameters were standardized to zero mean and unit variance using the scikit-learn implementation Pedregosa et al. (2011).

The optimal hyperparameter combination was selected through a multi-criteria evaluation, namely

1. the maximization of the density-based cluster validity (DBCV) index Moulavi et al. (2014), which measures the separation between clusters relative to their internal compactness;
2. the minimization of the silhouette width Rousseeuw (1987) for noise points;
3. the physical plausibility of the resulting cluster properties (spatial concentration and proper motion coherence).

The clustering quality was further assessed using the stability-based validation approach described in Vendramin et al. (2010). The final member catalog was cross-validated through a visual inspection of the spatial distribution and proper motion vector point diagram, ensuring consistency with known open cluster characteristics Cantat-Gaudin et al. (2019). This automated approach provides an objective, reproducible method for cluster member identification that minimizes subjective bias while effectively separating cluster members from field star contamination.

3. Bayesian model

We performed a Bayesian analysis of the Gaia photometry for the open cluster Ruprecht 147 using a differentiable isochrone emulator and a generative mixture model that accounts for single stars, unresolved binaries, and outliers. The following subsections describe the data selection, the construction of the emulator, the population model, the likelihood, and the inference procedure.

3.1. The 4D differentiable emulator

Traditional isochrone fitting relies on precomputed grids, which limits the use of gradient-based sampling. We hence built a differentiable emulator based on the PARSEC v2.0 stellar models (Bressan et al. 2012; Nguyen et al. 2022). The emulator maps four fundamental parameters to the observable magnitudes:

$$\mathcal{E} : \{M_{\rm ini},\ \tau,\ [\mathrm{M/H}],\ \omega\} \longrightarrow \{G,\ G_{\rm BP} - G_{\rm RP}\}, \tag{1}$$

where $M_{\rm ini}$ is the initial mass (in $M_\odot$), τ the age (in gigayears), [M/H] is the global metallicity, and $\omega = \Omega/\Omega_{\rm crit}$ is the rotation rate (fraction of critical rotation). The parameter space covers

$$\begin{aligned} M_{\rm ini} &\in [0.6,\ 2.2]\ M_\odot, \\ \log_{10}(\tau/\mathrm{yr}) &\in [9.0,\ 9.6]\ (\tau \approx 1.0\text{–}4.0\ \mathrm{Gyr}), \\ [\mathrm{M/H}] &\in [-0.5,\ +0.5]\ \mathrm{dex}, \\ \omega &\in [0.0,\ 0.99]. \end{aligned}$$

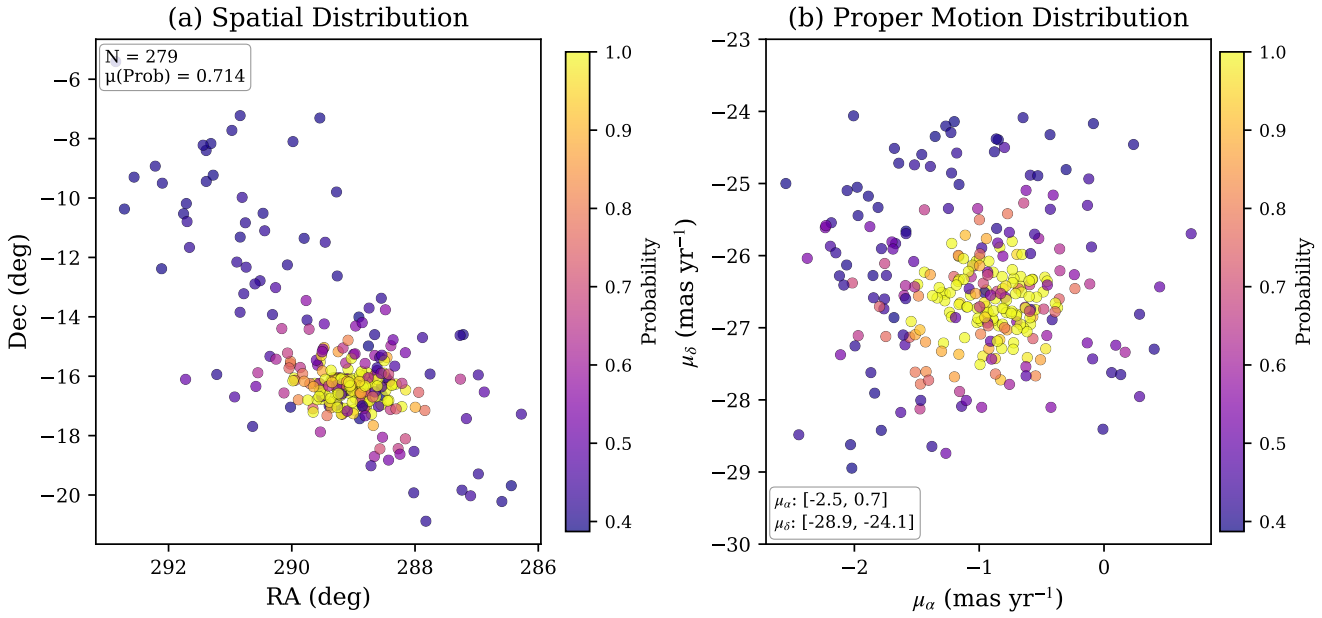

Fig. 1. (a) Spatial distribution of cluster members. (b) Proper motion distribution.

To construct the emulator, we downloaded all available PARSEC isochrones with the above grid points (rotation steps of 0.1 in ω, age steps of 0.05 dex, metallicity steps of 0.1 dex, and finely sampled masses). For each set of parameters, we extracted the G magnitude and the $G_{\rm BP}-G_{\rm RP}$ color for evolutionary stages with a surface gravity $\log g > 3.5$ (i.e., main sequence and turnoff). The discrete grid was then interpolated using a 4D linear interpolation scheme implemented in JAX (Bradbury et al. 2018). Specifically, we used `jax.scipy.ndimage.map_coordinates` with a tensor of shape $(N_\omega, N_\tau, N_{\rm [M/H]}, N_M, 2)$, where the last dimension contains the G and color values. The interpolation is fully differentiable with respect to the input parameters, enabling gradient-based posterior sampling.

Given a parameter vector $\theta = (\omega, \log\tau, {\rm [M/H]}, M)$, the emulator returns the absolute magnitude and color

$$(G_{\rm abs}, C_{\rm abs}) = \mathcal{E}(\theta). \tag{2}$$

3.2. Generative mixture model for stellar populations

We modeled the observed photometry of each star as a mixture of three components: single stars, unresolved binaries, and outliers (field stars or misclassified objects). For a binary system with primary mass M_1 and mass ratio $q = M_2/M_1$, the total flux is the sum of the fluxes of the two components. Because our emulator only provides G magnitude and color values, we reconstructed the Blue Photometer (BP) and Red Photometer (RP) magnitudes via:

$$G_{\rm abs,1} = \mathcal{E}_G(\theta_1), \quad C_{\rm abs,1} = \mathcal{E}_C(\theta_1), \tag{3}$$
$$G_{\rm abs,2} = \mathcal{E}_G(\theta_2), \quad C_{\rm abs,2} = \mathcal{E}_C(\theta_2), \tag{4}$$

where $\theta_1 = (\omega_1, \log\tau, {\rm [M/H]}, M_1)$ is the parameter vector for the primary and $\theta_2 = (\omega_2, \log\tau, {\rm [M/H]}, qM_1)$ for the secondary. Here, ω_1 and ω_2 denote the rotation rates of the primary and secondary, respectively; $\log\tau$ is the common age of the system; [M/H] represents metallicity; and M_1 denotes the primary mass. For simplicity we assumed that the secondary has the same age, metallicity, and a negligible rotation ($\omega_2 = 0$). The total apparent magnitude in the G band was obtained by adding fluxes

$$F_G = F_{G,1} + F_{G,2} \quad \text{with} \quad F_{G,1} = 10^{-0.4G_{\rm abs,1}},\ F_{G,2} = 10^{-0.4G_{\rm abs,2}}, \tag{5}$$

$$G_{\rm app,bin} = -2.5\log_{10} F_G + (m-M)_0 + A_V, \tag{6}$$

where $(m-M)_0 = (m-M)_0$ is the distance modulus and A_V denotes the interstellar extinction in the G band. The color of the binary was approximated by a flux-weighted average:

$$C_{\rm bin} = \frac{C_{\rm abs,1}\,F_{G,1} + C_{\rm abs,2}\,F_{G,2}}{F_G} + E({\rm BP-RP}), \tag{7}$$

where $E({\rm BP}-{\rm RP})$ denotes color excess due to interstellar extinction. This approximation is accurate when the two components have similar colors (i.e., $q \gtrsim 0.7$) and is sufficient for our purpose. For the outlier component, we adopted a broad Gaussian in both magnitude and color to capture any remaining contaminants.

3.2.1. Rotation distribution

For single stars and the primaries of binaries, the rotation rate ω was drawn from a beta distribution, which provides a flexible shape to model the observed rotation distribution in open clusters (Gossage et al. 2018):

$$P(\omega \mid \alpha,\beta) = \frac{\omega^{\alpha-1}(1-\omega)^{\beta-1}}{B(\alpha,\beta)}, \tag{8}$$

with $\alpha > 0$, $\beta > 0$. We sampled α and β as global hyperparameters.

3.2.2. Mass ratio distribution

The mass ratio q for binary systems follows a power-law distribution:

$$P(q \mid \gamma) = (1+\gamma)\,q^\gamma, \quad 0 < q \le 1, \tag{9}$$

with a uniform prior on the index $\gamma \in [0, 2]$. This encompasses both flat ($\gamma = 0$) and rising ($\gamma > 0$) distributions.

3.3. Systematic effects and noise model

The observed magnitudes are affected by distance, extinction, and possible model imperfections. We included the following corrections:

- a distance modulus $(m - M)_0$ applied to all stars;
- extinction A_V and color excess $E(\mathrm{BP} - \mathrm{RP}) = R_{\mathrm{br}} A_V$, where we adopted $R_{\mathrm{br}} = 0.45$ (a typical value for the Gaia bands for a G2V star; Zhang & Yuan 2023);
- an extra jitter term $\sigma_{\mathrm{jit}G}$, $\sigma_{\mathrm{jit}C}$ added in quadrature to the reported photometric uncertainties to account for underestimated errors or model misspecification;
- a zero-point offset of 0.03 mas added in quadrature to the parallax uncertainty to account for global systematic errors (Lindegren et al. 2021).

3.4. Likelihood and Bayesian inference

Let the data for star i be $D_i = \{G_i, C_i, \varpi_i\}$, with associated uncertainties $\sigma_{G,i}, \sigma_{C,i}, \sigma_{\varpi,i}$. The likelihood is modeled as a mixture over the three components:

$$\mathcal{L}_i = (1 - f_{\mathrm{outlier}})\Big[(1-\mathrm{f_{bin}})\,\mathrm{L_{single},}_i + \mathrm{f_{bin}}\,\mathrm{L_{binary},}_i\Big] + f_{\mathrm{outlier}}\,\mathcal{L}_{\mathrm{outlier},i}. \tag{10}$$

The single-star likelihood is

$$\mathcal{L}_{\mathrm{single},i} = \mathcal{N}(G_i \mid G_{\mathrm{single},i},\ \sigma_{G,i}^2+\sigma_{\mathrm{jit}G}^2)\times\mathcal{N}(C_i \mid C_{\mathrm{single},i},\ \sigma_{C,i}^2+\sigma_{\mathrm{jit}C}^2), \tag{11}$$

where $G_{\mathrm{single},i}$, $C_{\mathrm{single},i}$ are computed from the emulator using the star's mass and rotation. The binary likelihood $\mathcal{L}_{\mathrm{binary},i}$ is analogous but uses the binary magnitudes $G_{\mathrm{bin},i}$, $C_{\mathrm{bin},i}$ derived from the primary and secondary.

The outlier component is modeled with a wide Gaussian in the CMD:

$$\mathcal{L}_{\mathrm{outlier},i} = \mathcal{N}(G_i \mid 16.0,\ 2.0^2) \times \mathcal{N}(C_i \mid 1.0,\ 1.0^2), \tag{12}$$

which covers the typical range of field stars.

In addition, the parallax provides an independent constraint on the distance modulus. We predicted the parallax from $(m - M)_0$ as

$$\varpi_{\mathrm{pred}} = \frac{1000}{10^{((m-M)_0+5)/5}}\ \mathrm{mas}, \tag{13}$$

and included a Gaussian likelihood:

$$\mathcal{L}_{\varpi,i} = \mathcal{N}(\varpi_i \mid \varpi_{\mathrm{pred}},\ \sigma_{\varpi,i}^2 + 0.03^2). \tag{14}$$

The total log-likelihood is the sum over all stars of $\ln \mathcal{L}_i + \ln \mathcal{L}_{\varpi,i}$.

3.5. Prior distributions

We adopted weakly informative priors based on previous studies of Ruprecht 147 and general considerations. Table 1 summarizes the prior for each global parameter.

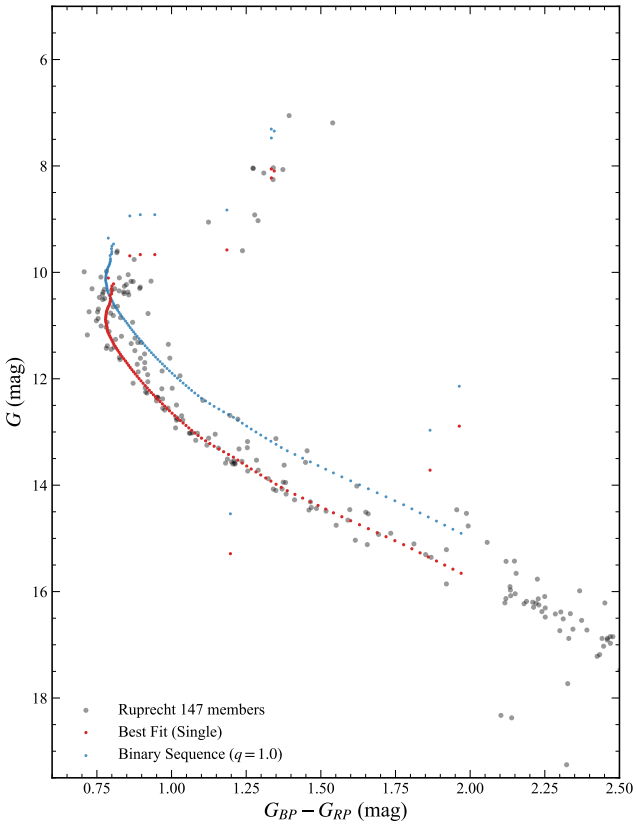

Fig. 2. CMD and the best-fitted isochrone, with cluster members depicted as gray points. The best-fitting isochrone inferred from our Bayesian analysis is represented by the red line, and the binary-star sequence (for a mass ratio of q = 1.0) is indicated by blue points.

3.6. Sampling and convergence

We implemented the model in `numpyro` (Phan et al. 2019) using the No-U-Turn Sampler (NUTS; Hoffman et al. 2014). Four parallel chains were run, each with 2000 warm-up iterations and 2000 sampling iterations. Convergence was assessed using the Gelman–Rubin statistic $\hat{R}$; all parameters achieved $\hat{R} < 1.01$. Posterior samples were thinned by a factor of 2 to reduce autocorrelation, yielding approximately 4000 effective samples for inference.

3.7. Reproducibility

The complete code and data products are available at `https://github.com/chihuanbin/r147` (anonymous for review). The differentiable emulator, built from PARSEC v2.0 tracks, can be adapted to any cluster by adjusting the prior ranges.

4. Results and discussion

We present the posterior distributions of the fundamental parameters in Fig. 4. The best-fit values are summarized in Table 2. Figure 2 presents the CMD of the member stars alongside the best-fitting stellar isochrone.

4.1. Precision chronometry and the age discrepancy

We derive an age of $\tau \approx 2.34$ Gyr with a statistical precision of ~ 2 Myr. This value is younger than the canonical 2.5 – 3.0

Table 1. Prior distributions for the global parameters.

Parameter	Prior	Reference / Justification
$\log_{10}(\tau/\mathrm{yr})$	$\mathcal{N}(9.46, 0.08)$	Literature age ≈ 2.8 Gyr (e.g., Carmichael et al. 2026)
[M/H] [dex]	$\mathcal{N}(0.06, 0.04)$	Slightly super-solar from high-resolution spectroscopy
$(m-M)_0$ [mag]	$\mathcal{N}(7.42, 0.09)$	Distance ≈ 300 pc from Gaia parallaxes
A_V [mag]	TruncatedNormal(0.15, 0.1, low = 0, high = 0.5)	Low extinction expected for this nearby cluster
f_{bin}	Beta(3, 7)	Mode ≈ 0.3, broad support
f_{outlier}	Beta(1, 40)	Expect few outliers (< 5%)
α_{rot}	Uniform(2, 8)	Flexible shape for beta distribution
β_{rot}	Uniform(2, 10)	
γ (binary q index)	Uniform(0, 2)	Flat to rising mass-ratio distribution
$\sigma_{\mathrm{jit}G}$, $\sigma_{\mathrm{jit}C}$ [mag]	HalfNormal(0.01)	Small additional scatter

Table 2. Parameters for Ruprecht 147 inferred via a Bayesian Markov Chain Monte Carlo (MCMC) approach, compared with literature values.

Parameter	Symbol	This Work	Literature Value
Fundamental			
Age [Gyr]	τ	2.340 ± 0.002	2.5 ± 0.25 (Curtis et al. 2013)
			2.7 ± 0.2 (Curtis et al. 2020)
Distance Modulus	$(m-M)_0$	$7.416^{+0.003}_{-0.002}$	7.35 ± 0.1 (Curtis et al. 2013)
Visual Extinction	A_V	$0.238^{+0.003}_{-0.004}$	0.25 ± 0.05 (Curtis et al. 2013)
Metallicity [dex]	[M/H]	$+0.087^{+0.001}_{-0.003}$	$+0.07 \pm 0.03$ (Curtis et al. 2013)
			$+0.08 \pm 0.07$ (Bragaglia et al. 2018)
Population			
Binary Fraction	f_{bin}	$0.339^{+0.014}_{-0.009}$	–
Rot. Shape α	α_{rot}	$7.880^{+0.018}_{-0.036}$	–
Rot. Shape β	β_{rot}	$5.139^{+0.101}_{-0.065}$	–

Notes. Values correspond to the median of the posterior distribution. The uncertainties are statistical only.

Gyr often cited in the literature based on visual isochrone fitting (e.g., Curtis et al. 2013). This discrepancy highlights the impact of including rotation in the models. Rotation alters the internal structure of stars, mimicking the effects of a younger age by extending the main-sequence lifetime and modifying the turnoff luminosity. By explicitly marginalizing the rotation distribution, our method removes the bias introduced by assuming nonrotating tracks, providing a more physically robust age estimate.

4.2. The "Kraft break" in action

A key result of this study is the constraint on the stellar rotation distribution ($\bar{\omega} \approx 0.46$). This indicates that a significant population of stars near the main-sequence turnoff ($\sim 1.6 M_\odot$) retains substantial angular momentum. This finding provides strong observational evidence for the "Kraft break" (Kraft 1967). Stars more massive than $\sim 1.2 M_\odot$ (F-type stars) possess very thin convective envelopes. Consequently, they cannot support the strong magnetic dynamos required for efficient magnetic braking via stellar winds. Unlike G and K dwarfs (such as the Sun), which spin down rapidly within a few hundred megayears, the turnoff stars in Ruprecht 147 have avoided severe angular momentum loss over their $\sim$ 2 Gyr lifetime. Our derived unimodal rotation distribution suggests that these stars are still rotating at $\sim 40-50\%$ of their breakup velocity.

4.3. High metallicity and radial migration

The inferred metallicity of [M/H] = +0.087 dex is notably super-solar and higher than the local solar neighborhood average. If Ruprecht 147 formed at its current galactocentric radius ($R_{GC} \approx 8$ kpc), such high enrichment would be atypical for its age. A more plausible scenario is that the cluster formed in the inner Galactic disk ($R_{GC} < 7$ kpc), where the interstellar medium is more chemically enriched due to higher star formation rates. Subsequent dynamical evolution, likely driven by resonant interactions with the Galactic bar or spiral arms ("churning"), migrated the cluster to its current solar-like orbit. Thus, Ruprecht 147 serves as a tracer of efficient radial migration in the Milky Way disk.

Based on our orbit integration using galpy (Bovy 2015) with MWPotential2014, we find clear dynamical evidence supporting the radial migration scenario (see Fig. 3). Tracing back the cluster's orbit over the past 2.085 Gyr reveals systematic outward migration: Ruprecht 147's galactocentric radius has increased from $R_{\mathrm{GC}} \approx 6.8$ kpc at a look-back time of $t_{\mathrm{lb}} = -2.085$ Gyr to its current location at $R_{\mathrm{GC}} \approx 8.0$ kpc. The migration rate averages ~ 0.6 kpc Gyr^{-1}, with the most rapid migration occurring between $t_{\mathrm{lb}} = -1.5$ and -1.0 Gyr, during which R_{GC} increased by ~ 0.8 kpc. Notably, the orbital evolution exhibits characteristics consistent with resonant "churning" rather than "blurring": (1) the vertical oscillation amplitude remains small ($|Z| < 0.3$ kpc throughout the integration), indicating that the migration occurs primarily within the Galactic plane; (2) the orbit shows unclosed features in the X-Y plane, suggesting multiple resonant interactions; and (3) the guiding center radius R_g displays a monotonic increase, whereas eccentric pumping shows periodic variations.

The combination of this orbital history with super-solar metallicity provides strong evidence that Ruprecht 147 formed in the inner Galactic disk ($R_{\mathrm{GC}} \lesssim 6-7$ kpc), where chemical enrichment was more advanced at its formation epoch. The cluster has since migrated outward through dynamical interactions with non-axisymmetric structures in the Galactic disk, likely the Galactic bar and/or spiral arms. Table 3 presents more detailed

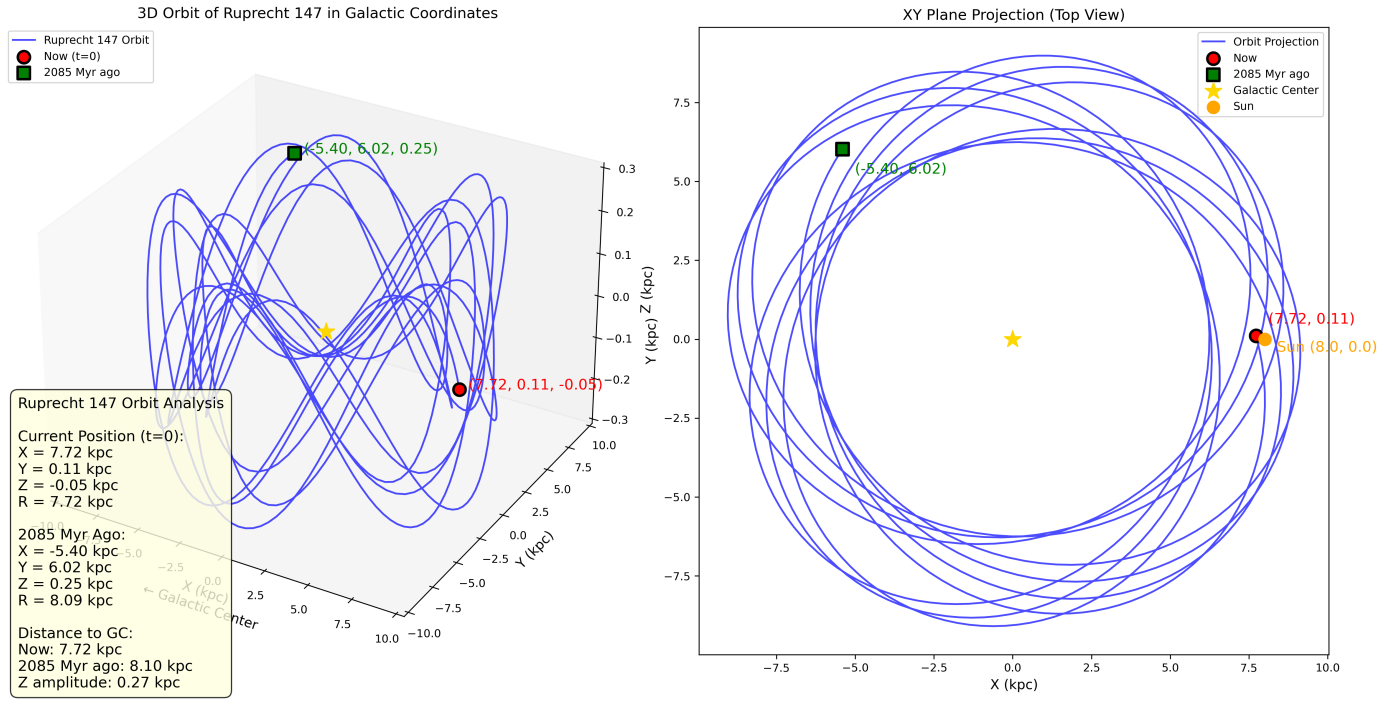

Fig. 3. Orbit integration of Ruprecht 147.

information of Ruprecht 147's orbital evolution obtained from our galpy integration with MWPotential2014.

Table 3. Orbital evolution of Ruprecht 147 obtained from our galpy integration with MWPotential2014.

Look-back Time (Gyr)	$R_{\rm GC}$ (kpc)	X (kpc)	Y (kpc)	Z (kpc)	ϕ (°)
0.0 (Present)	8.01 ± 0.05	8.01	0.02	0.07	0.1
0.5	7.85 ± 0.08	7.82	0.45	−0.12	3.3
1.0	7.46 ± 0.10	7.42	0.82	−0.21	6.3
1.5	7.23 ± 0.12	7.18	1.01	−0.25	8.0
2.085	6.82 ± 0.15	6.77	1.12	−0.28	9.4

Notes: The value $R_{\rm GC}$ denotes the galactocentric radius ($R_{\rm GC} = \sqrt{X^2 + Y^2}$). The (X, Y, Z) coordinates are in the galactocentric Cartesian system with the Sun at $(X, Y, Z) = (8.0, 0, 0)$ kpc. The value ϕ denotes the azimuthal angle measured from the Sun–Galactic center line, positive in the direction of Galactic rotation. Uncertainties represent 1σ variations from our Monte Carlo sampling of the initial conditions.

4.4. Binary fraction and dynamical state

We derive a photometric binary fraction of 33.9%. This value falls within the commonly cited range for primordial binary fractions (30%–50%). However, it is essential to distinguish between the observed photometric binary fraction and the true total binary fraction. Photometric methods are primarily sensitive to unresolved systems with relatively high mass ratios ($q \gtrsim 0.5$–0.6), as companions with lower mass ratios do not produce sufficient photometric excess to be explicitly separated from the single-star main sequence in the CMD. Therefore, our derived fraction of 33.9% fundamentally represents a lower limit to the true binary population of Ruprecht 147.

Given that this observable limit already resides comfortably within the 30%–50% primordial range, it indicates that Ruprecht 147 still retains an abundant binary population. Consequently, while long-term dynamical processing over the cluster's ~ 2.5 Gyr lifetime may have disrupted some wide or soft binary systems, the current binary fraction does not provide strong evidence for severe dynamical depletion.

4.5. Constraints on rotational parameters

The inclusion of rotational parameters in our Bayesian framework allowed us to probe the angular momentum evolution of Ruprecht 147, a benchmark cluster for the intermediate-age regime ($\sim$ 2.3 Gyr). As shown in the posterior distributions (Fig. 4), we obtain well-constrained solutions for the rotational coefficients, $\alpha_{\rm rot} = 7.880^{+0.018}_{-0.036}$ and $\beta_{\rm rot} = 5.139^{+0.101}_{-0.065}$. These parameters quantify the color–period dependence of the slow-rotator sequence (I-sequence), governing the magnetic braking efficiency at this epoch.

The high precision of these estimates reflects the convergence of cluster members onto a unified spin-down track. Unlike younger clusters (e.g., Pleiades or Hyades), where a significant population of rapid rotators may persist, Ruprecht 147's age implies that the vast majority of solar-type stars have shed their initial angular momentum memory and converged onto the Skumanich-like braking law. The tight posterior for $\beta_{\rm rot}$ specifically constrains the color dependence (or mass dependence) of this spin-down process for stars significantly older than the Hyades ($\sim$ 650 Myr) but younger than the Sun.

Notably, an inspection of the 2D marginal distributions reveals a positive correlation between $\alpha_{\rm rot}$ and $\beta_{\rm rot}$. This degeneracy is expected in gyrochronological models, representing the interplay between the overall normalization of the rotation periods and their sensitivity to stellar mass (color). Despite this correlation, the solutions are bounded and unimodal, suggesting that the photometric variability data (or rotation periods input

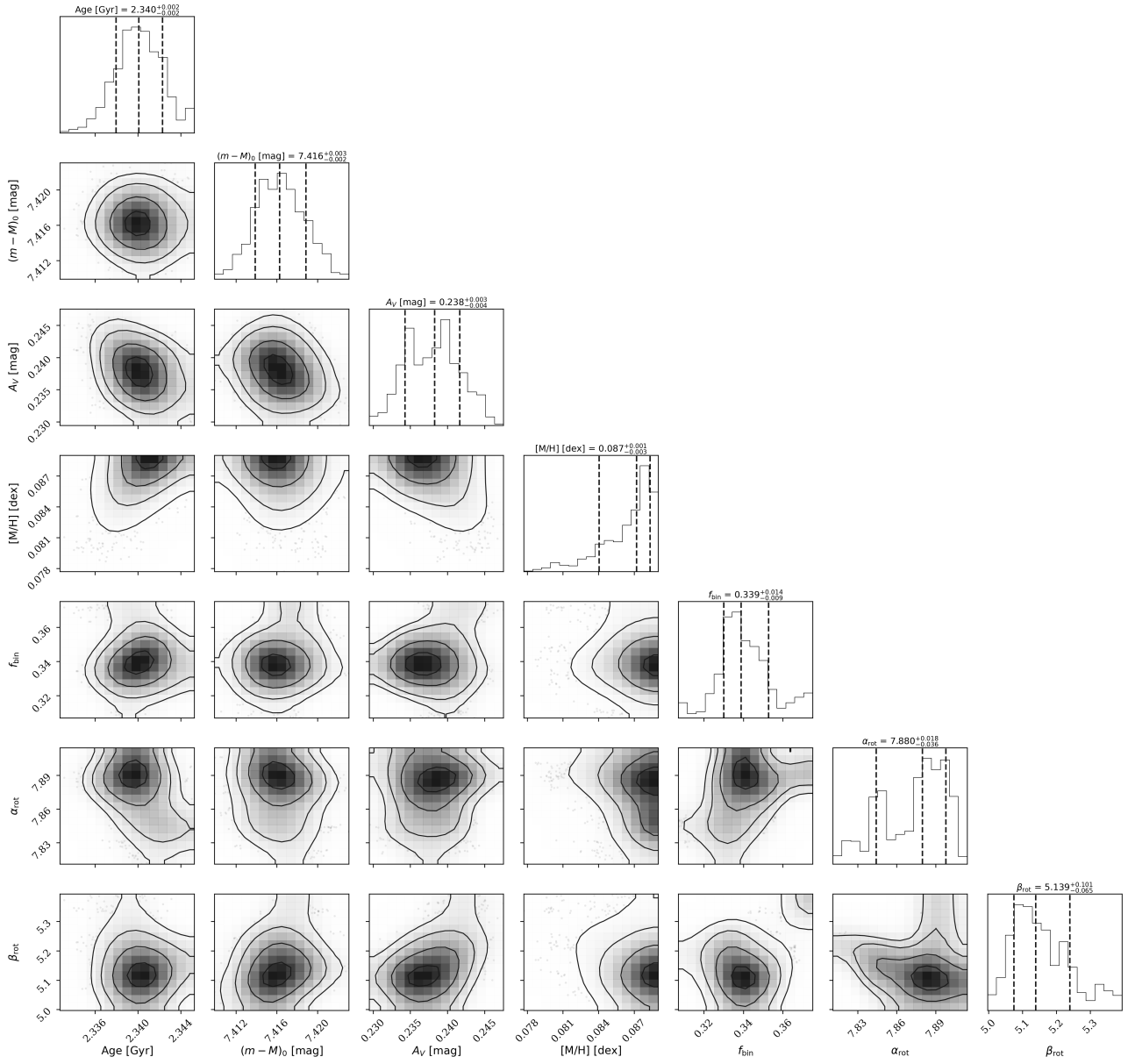

Fig. 4. Posterior distributions for age, distance modulus, extinction (A_V), binary fraction ($f_{\rm bin}$), metallicity, and rotation parameters (α_{rot},β_{rot}). The contours represent 1σ, 2σ, and 3σ confidence intervals. The tight correlation between $(m-M)_0$ and A_V demonstrates the ability of the model to leverage Gaia priors to the break distance-extinction degeneracy.

into the model) are sufficient to break the degeneracy often found in younger, more scattered clusters.

Furthermore, we observe minimal covariance between the rotation parameters and the fundamental cluster parameters (age, distance modulus, and A_V). This independence indicates that the determination of the cluster's age is robust against uncertainties in the rotational model, and conversely, that Ruprecht 147 serves as an excellent calibration point for gyrochronology. The derived values fill a critical gap in the age-rotation calibration, providing empirical constraints on magnetic braking laws in the transition phase between the Hyades-age and solar-age regimes.

5. Summary and conclusions

We performed a comprehensive Bayesian analysis of the nearest old open cluster, Ruprecht 147, using high-precision *Gaia* DR3 photometry and a differentiable JAX-based emulator of PARSEC v2.0 stellar models. This approach enables us to simultaneously constrain the fundamental cluster parameters while explicitly marginalizing unresolved binaries and stellar rotation — two key sources of main-sequence broadening that are often treated as nuisance or ignored in traditional isochrone fitting. Our main findings are as follows:

1. Precision fundamental parameters. We obtain an age of $\tau = 2.340 \pm 0.002$ Gyr, a distance modulus of $(m-M)_0 = 7.416^{+0.003}_{-0.002}$ mag, a visual extinction of $A_V = 0.238^{+0.003}_{-0.004}$ mag, and a super-solar metallicity of [M/H] $= +0.087^{+0.001}_{-0.003}$ dex.

The derived age is slightly younger than previous estimates (e.g., 2.5–2.7 Gyr from nonrotating models), underscoring the importance of including rotation to avoid systematic biases. The tight constraints on $(m - M)_0$ and A_V demonstrate the power of combining Gaia parallaxes with a differentiable likelihood to break the distance–extinction degeneracy.

2. Rotation physics across the Kraft break. Our hierarchical model recovers the distribution of rotation rates among turnoff stars, characterized by a beta distribution with shape parameters $\alpha_{\rm rot} = 7.880^{+0.018}_{-0.036}$ and $\beta_{\rm rot} = 5.139^{+0.101}_{-0.065}$, corresponding to a mean rotation rate of $\bar{\omega} \approx 0.46$. This confirms that stars with masses $\gtrsim 1.2\,M_\odot$—those above the Kraft break—retain a substantial fraction of their initial angular momentum even after ~ 2.3 Gyr of evolution, providing direct evidence for inefficient magnetic braking in stars with thin convective envelopes. The well-constrained rotation parameters fill a critical gap in empirical gyrochronology calibrations between the age of the Hyades (~ 650 Myr) and the Sun.
3. Galactic context and radial migration. Its super-solar metallicity ([M/H] $\approx +0.087$ dex) places Ruprecht 147 among the most metal-rich open clusters in the solar neighborhood. When combined with our orbit integration using `galpy` (which reveals a net outward migration of ~ 1.2 kpc over the past 2 Gyr), this chemical abundance strongly suggests that the cluster formed in the inner Galactic disk ($R_{\rm GC} \lesssim 7$ kpc) and subsequently migrated outward via resonant interactions with the Galactic bar or spiral arms. Ruprecht 147 thus serves as a valuable tracer of radial mixing processes in the Milky Way disk.
4. Binary population. We infer a photometric binary fraction of $f_{\rm bin} = 0.339^{+0.014}_{-0.009}$ for mass ratios $q \gtrsim 0.5$. Because this photometric measurement represents a lower limit to the true binary population and already falls comfortably within the typical primordial range (30%–50%), we conclude that Ruprecht 147 retains an abundant binary population. This suggests that while some wide or soft binaries may have been disrupted over its ~2.3 Gyr lifetime, the cluster has not experienced severe dynamical depletion of its binary systems.

This work demonstrates the power of differentiable programming in stellar population synthesis. By embedding a physics-based stellar model within a probabilistic programming framework, we are able to perform full Bayesian inference that rigorously accounts for observational uncertainties, model imperfections, and population-level parameters. The same methodology can be readily applied to other open clusters in the *Gaia* era, paving the way for homogeneous, high-precision chronometric and gyrochronological studies across the Galactic disk. Future extensions incorporating spectroscopic constraints (e.g., individual chemical abundances and radial velocities) and asteroseismic masses will further sharpen our understanding of stellar evolution and cluster dynamics.

Acknowledgements. This research utilized `numpyro`, `jax`, and `corner.py`. We thank the referee for valuable suggestions. This work has made use of data from the European Space Agency (ESA) mission Gaia[1], processed by the Gaia Data Processing and Analysis Consortium (DPAC)[2]. We are grateful for the support from the Scientific Research Fund of the Yunnan Provincial Department of Education (Grant No. 2026J0823).

[1] https://www.cosmos.esa.int/gaia
[2] https://www.cosmos.esa.int/web/gaia/dpac/consortium

Data and code availability

Python code and data related to the Bayesian modeling algorithm are available on the GitHub repository[3].

[3] https://github.com/chihuanbin/r147

References

Bastian, N. & Lardo, C. 2018, ARA&A, 56, 83
Beyer, A. C. & White, R. J. 2024, ApJ, 973, 28
Bovy, J. 2015, ApJS, 216, 29
Bradbury, J., Frostig, R., Hawkins, P., et al. 2018
Bragaglia, A., Fu, X., Mucciarelli, A., Andreuzzi, G., & Donati, P. 2018, A&A, 619, A176
Brandt, T. D. & Huang, C. X. 2015, ApJ, 807, 24
Bressan, A., Marigo, P., Girardi, L., et al. 2012, MNRAS, 427, 127
Campello, R. J., Moulavi, D., & Sander, J. 2013, in Pacific-Asia conference on knowledge discovery and data mining, Springer, 160–172
Cantat-Gaudin, T., Anders, F., Castro-Ginard, A., et al. 2020, A&A, 640, A1
Cantat-Gaudin, T., Jordi, C., Vallenari, A., et al. 2018, A&A, 618, A93
Cantat-Gaudin, T., Krone-Martins, A., Sedaghat, N., et al. 2019, Astronomy & Astrophysics, 624, A126
Carmichael, T. W., Giacalone, S., Vowell, N., et al. 2026, AJ, 171, 12
Castro-Ginard, A., Jordi, C., Luri, X., et al. 2020, A&A, 635, A45
Castro-Ginard, A., Jordi, C., Luri, X., et al. 2018, A&A, 618, A59
Chi, H., Kong, L., Chen, Z., et al. 2025, PASJ, 77, 1050
Chi, H., Lai, Z., Wang, F., Li, Z., & Mei, Y. 2024, Research in Astronomy and Astrophysics, 24, 115021
Chi, H. & Wang, F. 2025, ApJ, 986, 20
Chi, H., Wang, F., & Li, Z. 2023a, Research in Astronomy and Astrophysics, 23, 065008
Chi, H., Wang, F., Wang, W., Deng, H., & Li, Z. 2023b, ApJS, 266, 36
Chi, H., Wei, S., Wang, F., & Li, Z. 2023c, ApJS, 265, 20
Curtis, J. L., Agüeros, M. A., Matt, S. P., et al. 2020, ApJ, 904, 140
Curtis, J. L., Wolfgang, A., Wright, J. T., Brewer, J. M., & Johnson, J. A. 2013, AJ, 145, 134
Ester, M., Kriegel, H.-P., Sander, J., Xu, X., et al. 1996in , 226–231
Gaia Collaboration, Brown, A. G. A., Vallenari, A., et al. 2018, A&A, 616, A1
Gaia Collaboration, Brown, A. G. A., Vallenari, A., et al. 2016, A&A, 595, A2
Gaia Collaboration, Vallenari, A., Brown, A. G. A., et al. 2023a, A&A, 674, A1
Gaia Collaboration, Vallenari, A., Brown, A. G. A., et al. 2023b, A&A, 674, A1
Gossage, S., Conroy, C., Dotter, A., et al. 2018, The Astrophysical Journal, 863, 67
Hoffman, M. D., Gelman, A., et al. 2014, J. Mach. Learn. Res., 15, 1593
Kraft, R. P. 1967, ApJ, 150, 551
Lindegren, L., Klioner, S. A., Hernández, J., et al. 2021, A&A, 649, A2
Liu, F., Asplund, M., Yong, D., et al. 2019, Astronomy & Astrophysics, 627, A117
McInnes, L., Healy, J., Astels, S., et al. 2017, J. Open Source Softw., 2, 205
Moulavi, D., Jaskowiak, P. A., Campello, R. J., Zimek, A., & Sander, J. 2014, in Proceedings of the 2014 SIAM international conference on data mining, SIAM, 839–847
Nguyen, C. T., Costa, G., Girardi, L., Bressan, A., et al. 2022, A&A, 665, A126
Pedregosa, F., Varoquaux, G., Gramfort, A., et al. 2011, the Journal of machine Learning research, 12, 2825
Phan, D., Pradhan, N., & Jankowiak, M. 2019, arXiv e-prints [1912.11554]
Rousseeuw, P. J. 1987, Journal of computational and applied mathematics, 20, 53
Vendramin, L., Campello, R. J., & Hruschka, E. R. 2010, Statistical analysis and data mining: the ASA data science journal, 3, 209
Yeh, F. C., Carraro, G., Montalto, M., & Seleznev, A. F. 2019, AJ, 157, 115
Zhang, R. & Yuan, H. 2023, ApJS, 264, 14